AIAA JOURNAL
Vol. 36, No. 10, October 1998

# Numerical Simulation of the Generation of Axisymmetric Mode Jet Screech Tones

Hao Shen* and Christopher K. W. Tam†
*Florida State University, Tallahassee, Florida 32306-4510*

**An imperfectly expanded supersonic jet invariably radiates both broadband noise and discrete frequency sound called screech tones. Screech tones are known to be generated by a feedback loop driven by the large-scale instability waves of the jet flow. Inside the jet plume is a quasiperiodic shock cell structure. The interaction of the instability waves and the shock cell structure, as the former propagates through the latter, is responsible for the generation of the tones. Currently, there are formulas that can predict the tone frequency fairly accurately. However, there is no known way to predict the screech tone intensity. In this work, the screech phenomenon of an axisymmetric jet at low supersonic Mach number is reproduced by numerical simulation. The computed mean velocity profiles and the shock cell pressure distribution of the jet are found to be in good agreement with experimental measurements. The same is true with the simulated screech frequency. Calculated screech tone intensity and directivity at selected jet Mach number are reported. The present results demonstrate that numerical simulation using computational aeroacoustic methods offers not only a reliable way to determine the screech tone intensity and directivity but also an opportunity to study the physics and detailed mechanisms of the phenomenon by an entirely new approach.**

## I. Introduction

SUPERSONIC jet noise consists of three principal components[1]: the turbulent mixing noise, the broadband-shock-associated noise, and the screech tones. Screech tones are discrete frequency sound. At low supersonic Mach numbers, the screech tones are associated with the axisymmetric oscillations of the jet and radiate principally in the upstream direction. It has been known since the early work of Powell[2] that screech tones are generated by a feedback loop. Recent works show that the feedback loop is driven by the instability waves of the jet flow.[1] In the plume of an imperfectly expanded jet is a quasiperiodic shock cell structure. Figure 1 shows schematically the feedback loop. Near the nozzle lip where the jet mixing layer is thin and most receptive to external excitation, acoustic disturbances impinging on this area excite the instability waves. The excited instability waves, extracting energy from the mean flow, grow rapidly as they propagate downstream. After propagating a distance of four to five shock cells, the instability wave having acquired a large enough amplitude interacts with the quasiperiodic shock cells in the jet plume. The unsteady interaction generates acoustic radiation, part of which propagates upstream outside the jet. Upon reaching the nozzle lip region, the acoustic waves excite the mixing layer of the jet. This leads to the generation of new instability waves. In this way, the feedback loop is closed.

At the present time, there are reliable screech tone frequency prediction formulas.[1,3] However, there is no known way to predict tone intensity and directivity, even if it is entirely empirical. This is not surprising because the tone intensity is determined by the nonlinearities of the feedback loop.

The principal objective of the present work is to simulate the screech phenomenon numerically for low-supersonic-Mach-number jets. It will be shown that numerical simulation is an accurate method for predicting screech tone intensity and directivity. Numerical simulation of jet noise generation is not a straightforward undertaking. Tam[4] had earlier discussed some of the major computational difficulties anticipated in such an effort. First, the problem is characterized by very disparate length scales. For instance, the acoustic wavelength of the screech tone is over 20 times larger than the initial thickness of the jet mixing layer that supports the instability waves. Further, there is also a large disparity between the magnitude of the fluid particle velocity of the radiated sound and the velocity of the jet flow. Typically, they are five to six orders different. To be able to compute accurately the instability waves and the radiated sound, a highly accurate computational aeroacoustics algorithm with shock-capturing capability and a set of high-quality numerical boundary conditions are required.

In Sec. II, the mathematical model, the computation algorithm, and the grid design are discussed. Section III describes the various numerical boundary conditions used in the simulation. Section IV elaborates on the distribution of artificial selective damping incorporated in the computation algorithm. The artificial selective damping terms are for the elimination of the high-wave-number spurious waves. They have no effect on the low-wave-number component (the physical solution) of the computation. They help to maintain a high-quality numerical solution free from contamination by spurious waves and numerical instability. Comparisons between numerical results and experimental measurements are provided in Sec. V. These include the mean velocity profiles, the shock cell structure, the dependence of the screech tone frequency on jet Mach number, and screech tone intensity. Excellent agreements with experimental measurements are found. Computed directivities for the first two harmonics of the dominant screech tone will also be provided.

## II. Mathematical Model, Computation Scheme, and Grid Design

In this work, we are interested in simulating the axisymmetric mode jet screech in the jet Mach number range of 1.0–1.25. The axisymmetric mode is the dominant screech mode for axisymmetric jets from convergent nozzles at these Mach numbers. For this purpose, only two-dimensional computations in the $x$–$r$ plane, where $(r, \theta, x)$ are the cylindrical coordinates, are necessary.

### A. Mathematical Model

For an accurate simulation of jet screech generation, it is essential that the feedback loop be modeled and computed correctly. The important elements that form the feedback loop are the shock cell structure, the large-scale instability wave, and the feedback acoustic waves. Because turbulence in the jet plays only an indirect role in the feedback loop, no attempt is made here to resolve it computationally. However, turbulence in the mixing layer of the jet is

Received Nov. 3, 1997; presented as Paper 98-0283 at the AIAA 36th Aerospace Sciences Meeting and Exhibit, Reno, NV, Jan. 12–15, 1998; revision received May 22, 1998; accepted for publication June 11, 1998. 

*Graduate Student, Department of Mathematics.
†Distinguished Research Professor, Department of Mathematics. Associate Fellow AIAA.

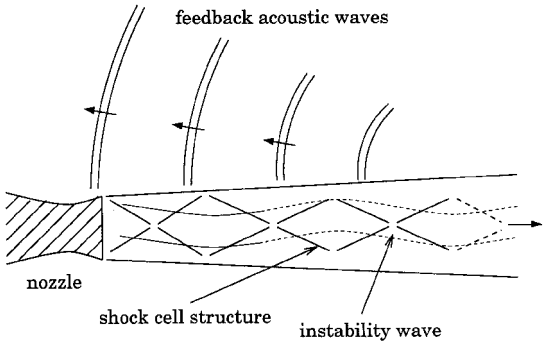


**Fig. 1 Schematic diagram of the screech tone feedback loop.**

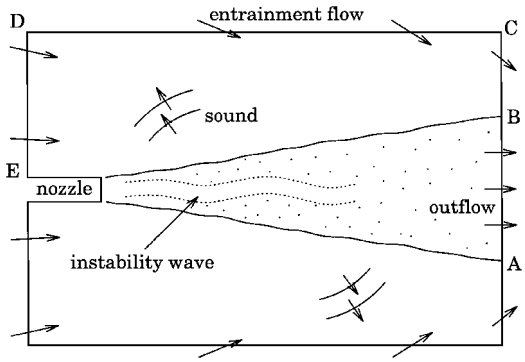


**Fig. 2 Physical domain to be simulated.**

responsible for its spreading, and the spreading rate of the jet affects the spatial growth and decay of the instability wave. To ensure a good simulation of the spreading rate, the $k$–$\varepsilon$ turbulence model is adopted. In the computation, the modified $k$–$\varepsilon$ model of Ref. 5, optimized for jet flows, is used.

Figure 2 shows the physical domain to be simulated. We will use length scale $= D$ (nozzle exit diameter), velocity scale $= a_\infty$ (ambient sound speed), timescale $= D/a_\infty$, density scale $= \rho_\infty$ (ambient gas density), pressure scale $= \rho_\infty a_\infty^2$, and temperature scale $= T_\infty$ (ambient gas temperature); scales for $k$, $\varepsilon$, and $\nu_t$ are $a_\infty^2$, $a_\infty^3/D$, and $a_\infty D$, respectively. The dimensionless governing equations in Cartesian tensor notation are

$$\frac{\partial \bar\rho}{\partial t} + \frac{\partial \bar\rho \tilde u_j}{\partial x_j} = 0 \tag{1}$$

$$\frac{\partial \bar\rho \tilde u_i}{\partial t} + \frac{\partial}{\partial x_j}(\bar\rho \tilde u_i \tilde u_j) = -\frac{\partial \bar p}{\partial x_i} - \frac{\partial}{\partial x_j}(\bar\rho \tau_{ij}) \tag{2}$$

$$\frac{\partial \bar\rho E}{\partial t} + \frac{\partial}{\partial x_j}(\bar\rho E \tilde u_j) = -\frac{\partial}{\partial x_j}(\bar p \tilde u_j) - \frac{\partial}{\partial x_j}(\bar\rho \tilde u_i \tau_{ij}) + \frac{1}{P_r(\gamma-1)}\frac{\partial}{\partial x_j}\left(\bar\rho \nu_t \frac{\partial \tilde T}{\partial x_j}\right) + \frac{1}{\sigma_k}\frac{\partial}{\partial x_j}\left(\bar\rho \nu_t \frac{\partial k}{\partial x_j}\right) \tag{3}$$

$$\frac{\partial \bar\rho k}{\partial t} + \frac{\partial}{\partial x_j}(\bar\rho k \tilde u_j) = -\bar\rho \tau_{ij}\frac{\partial \tilde u_i}{\partial x_j} - \bar\rho\varepsilon + \frac{1}{\sigma_k}\frac{\partial}{\partial x_j}\left(\bar\rho \nu_t \frac{\partial k}{\partial x_j}\right) \tag{4}$$

$$\frac{\partial \bar\rho \varepsilon}{\partial t} + \frac{\partial}{\partial x_j}(\bar\rho \varepsilon \tilde u_j) = -C_{\varepsilon 1}\frac{\varepsilon}{(k+k_0)}\bar\rho \tau_{ij}\frac{\partial \tilde u_i}{\partial x_j} - C_{\varepsilon 2}\frac{\bar\rho \varepsilon^2}{(k+k_0)} + \frac{1}{\sigma_\varepsilon}\frac{\partial}{\partial x_j}\left(\bar\rho \nu_t \frac{\partial \varepsilon}{\partial x_j}\right) \tag{5}$$

$$\gamma \bar p = \bar\rho \tilde T \tag{6}$$

$$E = \frac{\tilde T}{\gamma(\gamma-1)} + \frac{1}{2}\tilde u_i^2 + k \tag{7}$$

$$\tau_{ij} = \frac{2}{3}k\delta_{ij} - \nu_t\left(\frac{\partial \tilde u_i}{\partial x_j} + \frac{\partial \tilde u_j}{\partial x_i} - \frac{2}{3}\frac{\partial \tilde u_k}{\partial x_k}\delta_{ij}\right) \tag{8}$$

$$\nu_t = C_\mu \frac{k^2}{(\varepsilon+\varepsilon_0)} + \frac{\nu}{a_\infty D} \tag{9}$$

where $\gamma$ is the ratio of specific heats and $\nu$ is the molecular kinematic viscosity. The terms $k_0 = 10^{-6}$ and $\varepsilon_0 = 10^{-4}$ are small positive numbers to prevent the division by zero. The model constants[5] are taken to be

$$C_\mu = 0.0874, \qquad \sigma_k = 0.324, \qquad \sigma_\varepsilon = 0.377$$

$$C_{\varepsilon 1} = 1.4, \qquad C_{\varepsilon 2} = 2.02, \qquad P_r = 0.422$$

$$\nu/a_\infty D = 1.7 \times 10^{-6}$$

Note that, for the range of Mach number and jet temperature considered, the Pope and Sarkar corrections that are often added to the $k$–$\varepsilon$ model[5] are not necessary. Outside the jet flow, both $k$ and $\varepsilon$ are zero. On neglecting the molecular viscosity terms, the governing equations become the Euler equations.

In this work, solutions of the preceding set of equations are to be found numerically. For a given jet operating condition, the solution is to provide the shock cell structure in the jet plume, the mean flow as well as the instability wave in the mixing layer, and the acoustic field of the screech tone outside the jet.

### B. Computation Scheme and Grid Design

In this work, the seven-point stencil Dispersion-Relation-Preserving (DRP) scheme[4,6] is used to time-march the solution to a time periodic state corresponding to the screech cycle. The coefficients of the scheme, including those of the backward difference stencils, are given in Ref. 4 (the value of $a_3$ should be 0.0208431427703). The DRP scheme has proven to be nearly nondispersive over a wide band of wave numbers. In the acoustic region, the use of eight mesh points per wavelength would be adequate. This allows a fairly coarse grid to be used in the entire region outside the jet flow.

### C. Grid Design

The mixing layer of the jet is very thin. The smallest size grid is employed here to provide needed resolution of the jet shear layer and instability waves. Figure 3 shows the entire computation domain. The domain extends 5 diameters back from the nozzle exit and 35 diameters long in the $x$ direction. It is 17 diameters in the $r$ direction. A larger computational domain of $45D \times 25D$ was used at the beginning. Numerical experiments, however, showed that the smaller domain gave essentially identical results. The domain is divided into four blocks (or subdomains) as far as the grid size is concerned. In Fig. 3, these subdomains are separated by black lines. The black lines represent buffer regions of three mesh spacings. Because acoustic waves propagate with no preference in direction, square grids are used. The finest grid in the block right downstream of the nozzle exit has $\Delta x = D/64$. This block is enclosed by the next block with $\Delta x = D/32$, which, in turn, is enclosed by another block with $\Delta x = D/16$. The outermost block has $\Delta x = D/8$. In

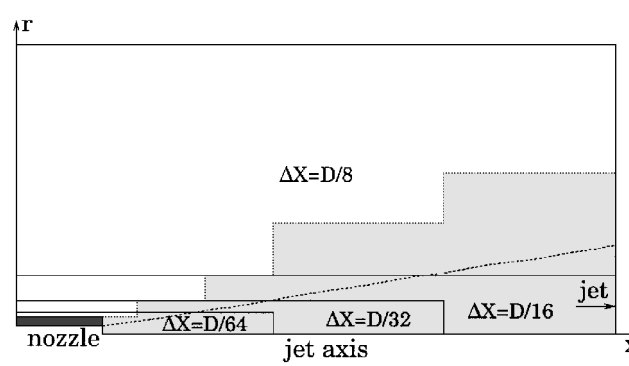


**Fig. 3 Computation domain in the $r$–$x$ plane showing the different subdomain and mesh sizes.**

Fig. 3, the dotted curve represents more or less the edge of the jet flow. This is well inside the lightly shaded region in which the governing equations are the $k$–$\varepsilon$ model turbulent flow equations. The full Euler equations are used in the unshaded region.

The buffer region is a narrow region around the boundaries of a computation subdomain of uniform size mesh. The change in the mesh size takes place in the buffer region. The basic design of the buffer region can be found in Ref. 7. In this work, a slightly improved version of the basic design is used.

## III. Numerical Boundary Conditions

Numerical boundary conditions play a crucial role in the simulation of the jet screech phenomenon. Recently an in-depth review of this subject was given by Tam.[8] For the present problem, several types of numerical boundary conditions are required. In Fig. 2, outflow boundary conditions are necessary along boundary AB. Along boundary BCDE, the radiation condition with entrainment flow is required. On the nozzle wall, the solid wall boundary condition is imposed. The jet flow is supersonic. So the inflow boundary condition can be prescribed at the nozzle exit plane. Finally, the equations of motion in cylindrical coordinates centered on the $x$ axis have an apparent singularity at the jet axis ($r \to 0$). A special treatment is needed to avoid the singularity computationally. In the following, a brief description of the different boundary conditions used in the simulations is provided.

### A. Radiation Boundary Conditions with Entrainment Flow

For accurate numerical simulation, the numerical boundary conditions to be imposed along boundary BCDE must perform three functions. First, they must specify the ambient conditions for the entire computation. This information is critical to the correct expansion of the jet and the development of the shock cell structure. Second, they must allow the acoustic waves generated to leave the computation domain with minimal reflection. Third, they must generate the entrainment flow induced by the jet. The development of such a set of radiation boundary conditions with entrainment flow is discussed in Ref. 8.

### B. Outflow Boundary Conditions

Along the outflow boundary AB, the mean flow is nonuniform. For this reason, the nonuniform outflow boundary conditions of Tam and Dong[9] are used. However, as the outflow boundary is only 30 jet diameters downstream, the instability wave amplitude, although damped at such a far distance, remains quite large. To allow for weak nonlinearities, we nonlinearized the outflow boundary conditions of Tam and Dong by replacing the linear terms by their nonlinear counterparts. In cylindrical coordinates, the complete set of outflow boundary conditions used is

$$\frac{\partial \rho}{\partial t} + u\frac{\partial \rho}{\partial x} + v\frac{\partial \rho}{\partial r} = \frac{1}{a^2}\left(\frac{\partial p}{\partial t} + u\frac{\partial p}{\partial x} + v\frac{\partial p}{\partial r}\right) \tag{10}$$

$$\frac{\partial u}{\partial t} + u\frac{\partial u}{\partial x} + v\frac{\partial u}{\partial r} = -\frac{1}{\rho}\frac{\partial p}{\partial x} \tag{11}$$

$$\frac{\partial v}{\partial t} + u\frac{\partial v}{\partial x} + v\frac{\partial v}{\partial r} = -\frac{1}{\rho}\frac{\partial p}{\partial r} \tag{12}$$

$$\frac{1}{V(\theta)}\frac{\partial p}{\partial t} + \cos\theta\frac{\partial p}{\partial x} + \sin\theta\frac{\partial p}{\partial r} + \frac{p-\bar{p}}{R} = 0 \tag{13}$$

$$\frac{\partial k}{\partial t} + u\frac{\partial k}{\partial x} + v\frac{\partial k}{\partial r} = 0 \tag{14}$$

$$\frac{\partial \varepsilon}{\partial t} + u\frac{\partial \varepsilon}{\partial x} + v\frac{\partial \varepsilon}{\partial r} = 0 \tag{15}$$

where $V(\theta) = u\cos\theta + a(1 - M^2\sin^2\theta)^{1/2}$ and $M = u/a$. The term $a$ is the speed of sound, and $(\theta, R)$ are spherical polar coordinates (the $x$ axis is the polar axis); the origin of $R$ has been taken to be at the end of the potential core of the jet. The last two of the preceding equations are the nonlinearized form of the linear asymptotic $k$–$\varepsilon$ equations (without sources). The term $\bar{p}$ is the static pressure calculated by the entrainment flow model at the edge of the jet flow at the outflow boundary.

### C. Inflow Boundary Conditions

At the nozzle exit plane, the flow variables are taken to be uniform, corresponding to those at the exit of a convergent nozzle. In addition, both $k$ and $\varepsilon$ are assumed to be zero. In other words, the mixing layer is regarded to be very thin. Thies and Tam,[5] in their jet mean flow calculation work, found that this is a reasonably good way to initiate the computation. For cold jets, the mixing layer evolves rapidly into a quasisimilar state resembling that in a physical experiment.

### D. Boundedness Treatment at the Jet Axis

In cylindrical coordinates, the governing equation has an apparent singularity at the jet axis ($r \to 0$). Reference 8 discusses two ways to treat this problem. In the present work, the governing equations are not used at $r = 0$. Instead, the formal limit of these equations as $r \to 0$ is used. Our experience is that this can be implemented in a straightforward manner by extending the seven-point stencil into the negative region of $r$. The flow variables $\rho$, $p$, and $u$ in the $r < 0$ region are determined by symmetric extension about the jet axis, whereas $v$ is obtained by an antisymmetric extension. These are the proper extensions for axisymmetric jet screech oscillations.

### E. Wall Boundary Conditions

On the nozzle wall, the boundary condition of no through flow is implemented by the ghost point method of Tam and Dong.[10] For the purpose of eliminating the generation of spurious waves, extra amounts of artificial selective damping are imposed around the nozzle wall region. By judging from the computed results, this is an effective way to avoid the generation of short spurious waves.

## IV. Artificial Selective Damping

The DRP scheme is a central difference scheme and, therefore, has no intrinsic dissipation. For the purpose of eliminating spurious short waves and to improve numerical stability, artificial selective damping terms[11] are added to the discretized finite difference equations.

In the interior region, the seven-point damping stencil[4] (with half-width $\sigma = 0.2\pi$) is used. An inverse mesh Reynolds number [$R_\Delta^{-1} = \nu_a/(a_\infty \Delta_x)$, where $\nu_a$ is the artificial kinematic viscosity] of 0.05 is prescribed over the entire computation domain. This is to provide general background damping to eliminate possible propagating spurious waves. Near the boundaries of the computation domain where a seven-point stencil does not fit, the five- and three-point damping stencils given in Ref. 4 are used.

Spurious numerical waves are usually generated at the boundaries of a computation domain. The boundaries are also favorite sites for the occurrence of numerical instability. This is true for both exterior boundaries as well as internal boundaries such as the nozzle walls and buffer regions where there is a change in mesh size. To suppress both the generation of spurious numerical waves and numerical instability, additional artificial selective damping is imposed along these boundaries. Along the inflow (radiation) and outflow boundaries, a distribution of inverse mesh Reynolds number in the form of a Gaussian function with a half-width of four mesh points (normal to the boundary) and a maximum value of 0.1 right at the outermost mesh points is incorporated into the time-marching scheme. Adjacent to the jet axis, a similar addition of artificial selective damping is implemented with a maximum value of the inverse mesh Reynolds number at the jet axis set equal to 0.35. On the nozzle wall, the use of a maximum value of additional inverse mesh Reynolds number of 0.2 has been found to be very satisfactory.

The two sharp corners of the nozzle lip and the transition point between the use of the outflow and the radiation boundary condition on the right side of the computation domain are locations requiring further additional numerical damping. This is done by adding a Gaussian distribution of damping around these special points.

As shown in Fig. 3, the four computation subdomains are separated by buffer regions. Here additional artificial selective damping is added to the finite difference scheme. In the supersonic region downstream of the nozzle exit, a shock cell structure develops in

the jet flow. To provide the DRP scheme with shock-capturing capability, the variable stencil Reynolds number method of Tam and Shen[12] is adopted. The jet mixing layer in this region has very large velocity gradient in the radial direction. Because of this, the $U_{\text{stencil}}$ of the variable stencil Reynolds number method is determined by searching over the seven-point stencil in the axial direction and only the two immediately adjacent mesh points in the radial direction. An inverse stencil Reynolds number distribution of the form

$$R^{-1}_{\text{stencil}} = 4.5F(x)G(r) \tag{16}$$

where

$$F(x) = \begin{cases} 1, & 0 \le x \le 9 \\ \exp\left[-\dfrac{\ell n\, 2}{(8\Delta x)^2}(x-9)^2\right], & 9 < x \end{cases}$$

$$G(r) = \begin{cases} 1, & 0 \le r \le 0.8 \\ \exp\left[-\dfrac{\ell n\, 2}{(4\Delta x)^2}(r-0.8)^2\right], & 0.8 < r \end{cases}$$

is used in all of the numerical simulations. It is possible to show, based on the damping curve ($\sigma = 0.3\pi$), that the variable damping has a minimal effect on the instability wave of the feedback loop. Also, extensive numerical experimentations indicate that the method used can, indeed, capture the oscillatory shocks in the jet plume and that the time-averaged shock cell structure compares favorably with experimental measurements.

## V. Numerical Results and Comparisons with Experiments

We have been able, using the numerical algorithm described earlier, to reproduce the jet screech phenomenon computationally. Figure 4 shows the computed density field in the $x$–$r$ plane at one instance after the initial transient disturbances have propagated out of the computational domain. The screech feedback loop locks itself into a periodic cycle without external interference. As can be seen, sound waves of the screech tone are radiated out in a region around the fourth to fifth shock cells downstream of the nozzle exit. Most of the prominent features of the numerically simulated jet screech phenomenon are in good agreement with physical experiments.[13–15]

### A. Mean Velocity Profiles and Shock Cell Structure

To demonstrate that the present numerical simulation can actually reproduce the physical experiment, we will first compare the mean flow velocity profile of the simulated jet with experimental measurements. For this purpose, the time-averaged velocity profiles of the axial velocity of a Mach 1.2 jet from one diameter downstream of the nozzle exit to seven diameters downstream at one-diameter intervals are measured from the numerical simulation. They are shown as a function of $\eta^* = (r - r_{0.5})/x$ in Fig. 5, where $r_{0.5}$ is the radial distance from the jet axis to the location where the axial velocity is

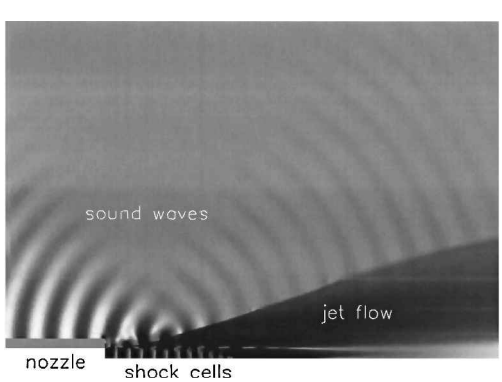


**Fig. 4 Density field from the numerical simulation showing the generation and radiation of the screech tone associated with a Mach 1.13, cold supersonic jet from a convergent nozzle.**

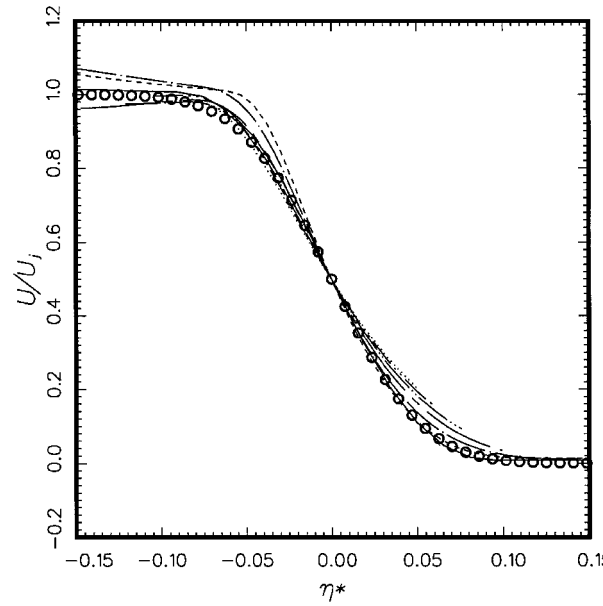


**Fig. 5 Comparison between mean velocity profiles of numerical simulation at $M_j$ = 1.2: ——, $x/D$ = 1.0; - - -, $x/D$ = 2.0; —·—, $x/D$ = 3.0; —·—, $x/D$ = 4.0; —··—, $x/D$ = 5.0; —·-·—, $x/D$ = 6.0; · · · · ·, $x/D$ = 7.0; $U/U_j = 0.5[1 - \text{erf}(\sigma\eta^*)]$; and ○, $\sigma$ = 17 from experiment.[16]**

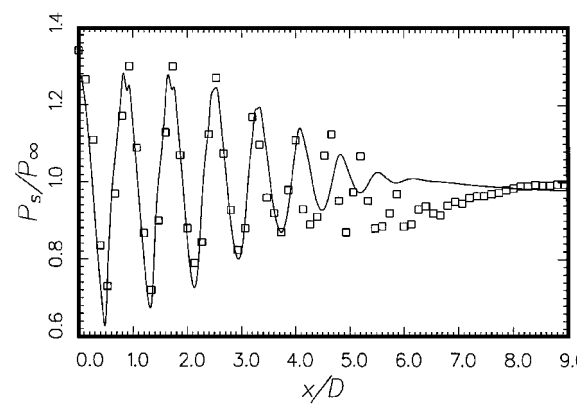


**Fig. 6 Comparison between calculated time-averaged pressure distribution along the centerline of a Mach 1.2 cold jet and the measurement of Norum and Brown[17]: ——, simulation, and □, experiment.**

equal to half the fully expanded jet velocity. Numerous experimental measurements have shown that the mean velocity profile when plotted as a function of $\eta^*$ would nearly collapse into a single curve. The single curve is well represented by an error function in the form

$$u/u_j = 0.5[1 - \text{erf}(\sigma\eta^*)] \tag{17}$$

where $\sigma$ is the spreading parameter. Extensive jet mean flow data had been measured by Lau.[16] By interpolating the data of Lau to Mach 1.2, it is found that experimentally $\sigma$ is nearly equal to 17.0. The empirical fit, formula (17), with $\sigma = 17.0$ is also plotted in Fig. 5 (the circles). As can readily be seen, there is good agreement between the empirical mean velocity profile and the profiles of the numerical simulation.

One important component of the screech feedback loop is the shock cell structure inside the jet plume. To ensure that the simulated shock cells are the same as those in an actual experiment, we compare the time-averaged pressure distribution along the centerline of the simulated jet at Mach 1.2 with the experimental measurements of Norum and Brown.[17] Figure 6 is a plot of the simulated and measured pressure distribution as a function of downstream distance. It is clear that the first five shocks of the simulation are in good agreement with experimental measurements in terms of both shock cell spacing and amplitude. Beyond the fifth shock cell, the

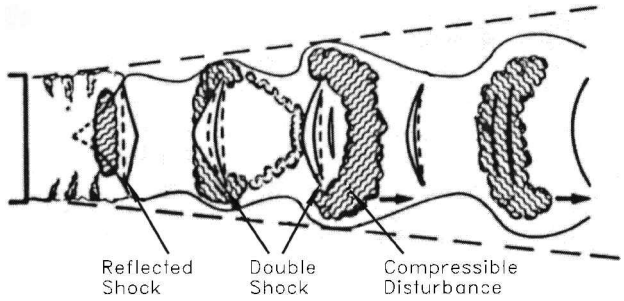


a) Experimental observation by Westley and Woolley[13]

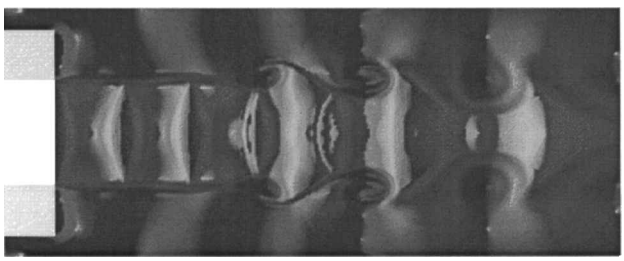

b) Numerical simulation

**Fig. 7 Unsteady shock cell structure and large-scale disturbances inside the jet plume at an instant.**

agreement is less good. At this time, we are unable to determine the cause of the discrepancy (including possible experimental error). However, it is known that screech tones are generated around the fourth shock cell. Therefore, any minor discrepancies downstream of the fifth shock cell would not invalidate our screech tone simulation.

During a screech cycle, the shock cell is not stationary. In the past, Westley and Woolley[13] had made extensive high-speed stroboscopic schlieren observations of the motion of the shock cells and the disturbances/instability wave in the mixing layer of the jet. Figure 7a is their sketch of the prominent features inside the jet plume. Figure 7b is the density field in a plane cutting through the centerline of the simulated jet. In comparing Figs. 7a and 7b one must be aware that the lighting in schlieren observation gives an integrated view of the density field across the jet. Despite this inherent difference, there are remarkable similarities between the two figures. Not only are the gross features of the large turbulence structure (in the form of toroidal vortices) and shock cells alike, but also the detailed features of the curved shocks are nearly the same. Based on the aforementioned comparisons, it is believed that the numerical simulation, indeed, can reproduce all of the important elements of the screech phenomenon.

### B. Screech Tone Frequency and Intensity

It is well known that at low supersonic jet Mach numbers there are two axisymmetric screech modes: the $A_1$ and the $A_2$ modes. Earlier, Norum[14] had compared the frequencies of the $A_1$ and $A_2$ modes measured by a number of investigators. His comparison indicates that the screech frequencies and the Mach number at which the transition from one mode to the other takes place (staging) vary slightly from experiment to experiment. It is generally agreed among experimentalists that the screech phenomenon is extremely sensitive to minor details of the experimental facility and jet operating conditions.

In the present numerical simulation, both the $A_1$ and $A_2$ axisymmetric screech modes are reproduced. Figure 8 shows the variation of $\lambda/D$, where $\lambda$ is the acoustic wavelength of the tone, with jet Mach number obtained by the present numerical simulation. Because $\lambda/D = a_\infty/(fD)$, where $f$ is the screech frequency, this figure essentially provides the frequency Mach number relationship. Also plotted are the measurements of Ponton and Seiner.[15] The data from both the numerical simulation and the experiment fall on the same two curves, one for the $A_1$ mode and the other for the $A_2$ mode. This suggests that the calculated screech frequencies are in complete agreement with experimental measurements,

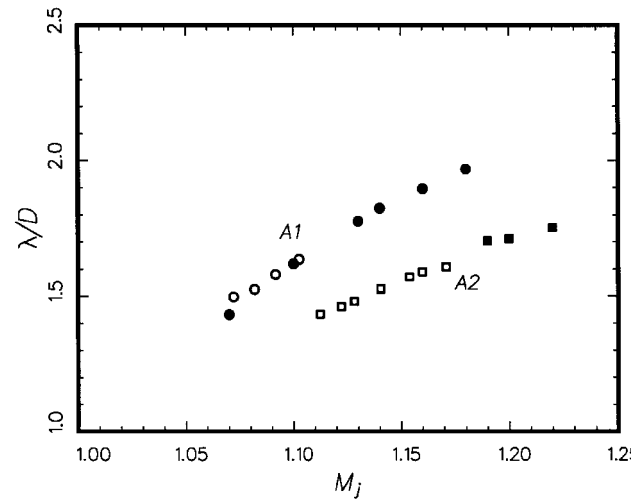


**Fig. 8 Comparison between the acoustic wavelengths of simulated screech tones and the measurements of Ponton and Seiner[15]: ○ and □, measurements, and ● and ■, simulation.**

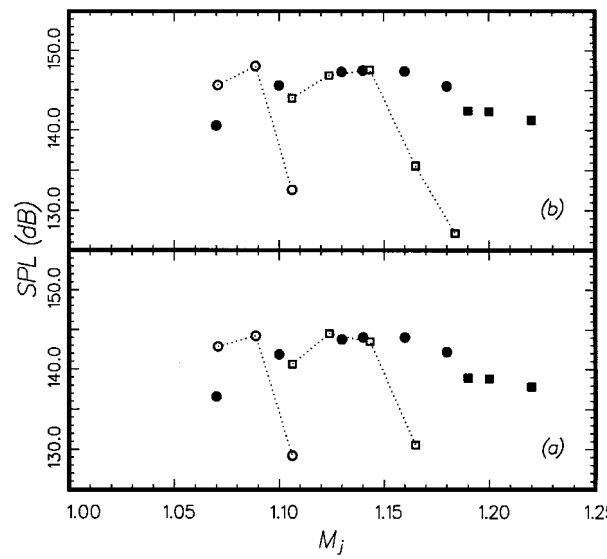


**Fig. 9 Intensity of axisymmetric screech tones at the nozzle exit plane: a) $r/D = 0.889$ and b) $r/D = 0.642$. Experiment [15]: ○, $A_1$ mode, and □, $A_2$ mode. Numerical simulation: ●, $A_1$ mode, and ■, $A_2$ mode.**

although the Mach number at which staging takes place is not the same.

Ponton and Seiner[15] mounted two pressure transducers at radial distances of $0.642D$ and $0.889D$, respectively, on the surface of the nozzle lip in their experiment. By means of these transducers, they were able to measure the intensities of the screech tones. Their measured values are plotted in Figs. 9a and 9b. The transducer of Fig. 9b is closer to the jet axis and hence shows a higher decibel level. Also plotted are the corresponding tone intensities measured in the numerical simulation. The peak levels of both physical and numerical experiments are nearly equal. Thus, except for the difference in the staging Mach number, the present numerical simulation is, indeed, capable of providing accurate screech tone intensity prediction as well.

### C. Directivity

The directivity patterns of the simulated screech tones have been measured. Typical directivities for the $A_1$ and $A_2$ modes are shown in Figs. 10 and 11. A search through the literature failed to find directivity measurements for the axisymmetric mode screech tones. Validation of these results, therefore, cannot be carried out at this time.

Figure 10a shows the directivity of the $A_1$ screech mode (fundamental frequency) at jet Mach number 1.18 scaled to a distance of

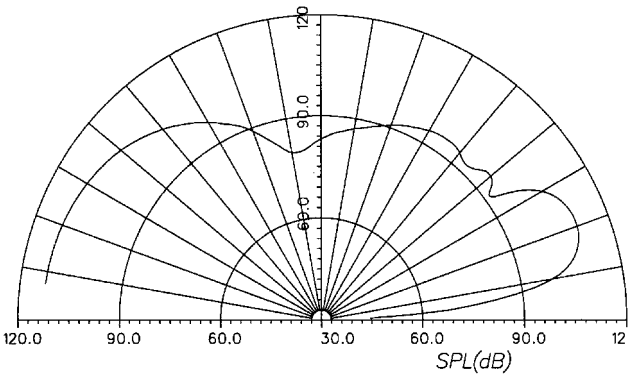


**a) Fundamental frequency**

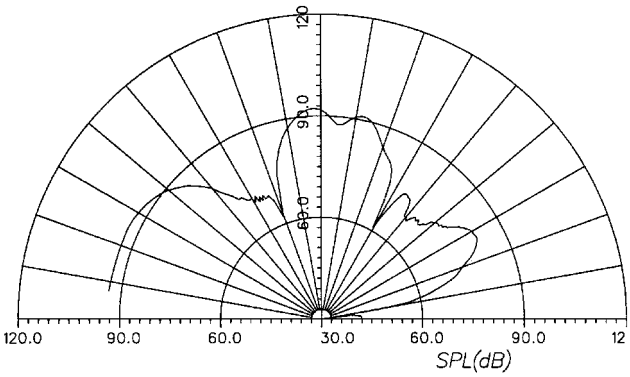


**b) Second harmonic**

**Fig. 10 Directivity of the $A_1$ mode screech tone at $M_j = 1.18$ and $r = 65D$.**

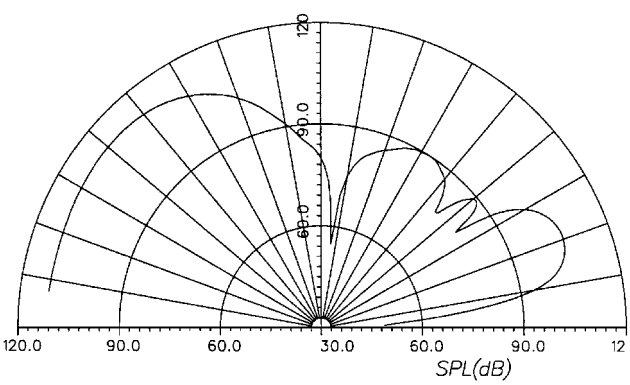


**a) Fundamental frequency**

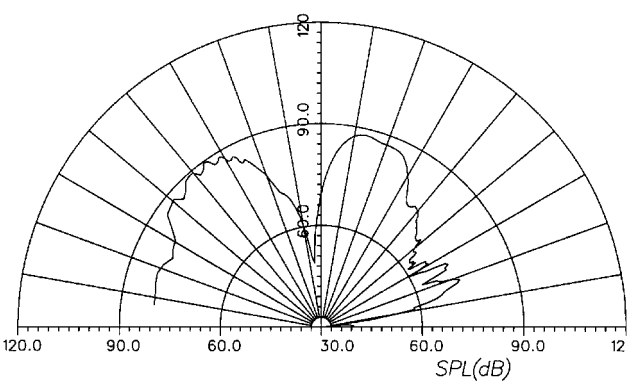


**b) Second harmonic**

**Fig. 11 Directivity of the $A_2$ mode screech tone at $M_j = 1.2$ and $r = 65D$.**

$65D$. The directivity of the second harmonic is given in Fig. 10b. Those for the $A_2$ mode at Mach 1.2 are shown in Figs. 11a and 11b. Overall, the directivity patterns of the $A_1$ and $A_2$ modes are similar. However, there are differences in detailed features. For the fundamental tone, the directivity pattern consists of two principal lobes. One lobe radiates upstream and forms part of the screech feedback loop. The other radiates downstream peaked at a relatively small angle from the jet flow direction. This is not sound generated by the interaction of instability wave and shock cells. It is Mach wave radiation generated directly by the instability wave as it propagates down the jet column.[1,18]

The directivity pattern of the second harmonic (Figs. 10b and 11b) also displays two principal lobes. One lobe peaks around the 90-deg direction. This is the principal lobe. The sound is generated by the nonlinearities of the source (nonlinear instability wave shock cell interaction). The other lobe is in the upstream direction. We believe this is generated by the nonlinear propagation effect of the upstream propagating feedback acoustic waves. The screech tone intensity is quite high. This leads immediately to wave steepening and the generation of harmonics. An examination of the waveforms measured at upstream locations confirms that they are not sinusoidal but somewhat distorted. Thus the main lobes of the second harmonic have entirely different origins.

## VI. Concluding Remarks

Recently, rapid advances have been made in the development of computational aeroacoustic methods. In this work, we have demonstrated that it is now possible to perform accurate numerical simulation of the jet screech phenomenon by the use of one of these methods, namely, the DRP scheme with artificial selective damping. Numerical boundary conditions are also crucial to the success of the simulations. At the present time, such numerical boundary conditions are available in the literature. In a previous review,[4] it was pointed out that, unlike traditional computational fluid dynamics problems, numerical simulation of jet noise generation is subjected to the difficulties of large length scale disparity and the need to resolve the many-order-of-magnitude differences in sound and flow. This work indicates that these problems can be overcome by a careful design of the computation grid and the use of an optimized high-order finite difference scheme.

The present work is restricted to the low-supersonic-Mach-number range for which the screech tones are axisymmetric. Future plans call for the extension of the work to three dimensions to allow the simulation of flapping modes at higher Mach numbers.

## Acknowledgments

This work was supported by Steven H. Walker at the U.S. Air Force Wright Laboratory under Delivery Order F33615-96-D-3011. The second author also wishes to acknowledge partial support from NASA Langley Research Center under Grant NAG 1-1776. Supercomputing time was provided by the U.S. Air Force Wright Laboratory, the SP2 computer of the Supercomputer Research Institute, and the Silicon Graphics Power Challenge computer of Florida State University.

## References

[1] Tam, C. K. W., "Supersonic Jet Noise," *Annual Review of Fluid Mechanics*, Vol. 27, 1995, pp. 17–43.

[2] Powell, A., "On the Mechanism of Choked Jet Noise," *Proceedings of the Physical Society, London*, Vol. 66, 1953, pp. 1039–1056.

[3] Tam, C. K. W., Shen, H., and Raman, G., "Screech Tones of Supersonic Jets from Bevelled Rectangular Nozzles," *AIAA Journal*, Vol. 35, No. 7, 1997, pp. 1119–1125.

[4] Tam, C. K. W., "Computational Aeroacoustics: Issues and Methods," *AIAA Journal*, Vol. 33, No. 10, 1995, pp. 1788–1796.

[5] Thies, A. T., and Tam, C. K. W., "Computation of Turbulent Axisymmetric and Nonaxisymmetric Jet Flows Using the $k$–$\varepsilon$ Model," *AIAA Journal*, Vol. 34, No. 2, 1996, pp. 309–316.

[6] Tam, C. K. W., and Webb, J. C., "Dispersion-Relation-Preserving Finite Difference Schemes for Computational Acoustics," *Journal of Computational Physics*, Vol. 107, Aug. 1993, pp. 262–281.

[7] Dong, Z., "Fundamental Problems in Computational Acoustics," Ph.D. Thesis, Dept. of Mathematics, Florida State Univ., Tallahassee, FL, Spring 1994.

[8]Tam, C. K. W., "Advances in Numerical Boundary Conditions for Computational Aeroacoustics," AIAA Paper 97-1774, June 1997; see also *Journal of Computational Acoustics* (to be published).

[9]Tam, C. K. W., and Dong, Z., "Radiation and Outflow Boundary Conditions for Direct Computation of Acoustic and Flow Disturbances in a Nonuniform Mean Flow," *Journal of Computational Acoustics*, Vol. 4, June 1996, pp. 175–201.

[10]Tam, C. K. W., and Dong, Z., "Wall Boundary Conditions for High-Order Finite Difference Schemes in Computational Aeroacoustics," *Theoretical and Computational Fluid Dynamics*, Vol. 8, Oct. 1994, pp. 303–322.

[11]Tam, C. K. W., Webb, J. C., and Dong, Z., "A Study of the Short Wave Components in Computational Acoustics," *Journal of Computational Acoustics*, Vol. 1, March 1993, pp. 1–30.

[12]Tam, C. K. W., and Shen, H., "Direct Computation of Nonlinear Acoustic Pulses Using High-Order Finite Difference Schemes," AIAA Paper 93-4325, Oct. 1993.

[13]Westley, R., and Woolley, J. H., "An Investigation of the Near Noise Fields of a Choked Axisymmetric Air Jet," *Proceedings of AFOSR-UTIAS Symposium on Aerodynamic Noise*, Univ. of Toronto Press, Toronto, ON, Canada, 1968, pp. 147–167.

[14]Norum, T. D., "Screech Suppression in Supersonic Jets," *AIAA Journal*, Vol. 21, No. 2, 1983, pp. 235–240.

[15]Ponton, M. K., and Seiner, J. M., "The Effects of Nozzle Exit Lip Thickness on Plume Resonance," *Journal of Sound and Vibration*, Vol. 154, No. 3, 1992, pp. 531–549.

[16]Lau, J. C., "Effects of Exit Mach Number and Temperatures on Mean-Flow and Turbulence Characteristics in Round Jets," *Journal of Fluid Mechanics*, Vol. 105, 1981, pp. 193–218.

[17]Norum, T. D., and Brown, M. C., "Simulated High-Speed Flight Effects on Supersonic Jet Noise," AIAA Paper 93-4388, Oct. 1993.

[18]Tam, C. K. W., and Burton, D. E., "Sound Generated by Instability Waves of Supersonic Flows: Part 1, Two Dimensional Mixing Layers; Part 2, Axisymmetric Jets," *Journal of Fluid Mechanics*, Vol. 135, 1984, pp. 249–295.

S. Glegg
*Associate Editor*